crystals

MDPI

Article

Polymorphism *vs.* Aromaticity in Cathinone Derivative 2-Amino-1-(4-Bromo-2,5-Dimethoxyphenyl)Ethan-1-One (bk-2C-B)

Natalina Makieieva [1,*], Teobald Kupka [2] and Krzysztof Ejsmont [2]

[1] Department of Physics, Faculty of Production Engineering and Logistics, Opole University of Technology, 31, K. Sosnkowskiego Street, 45-272 Opole, Poland
[2] Faculty of Chemistry and Pharmacy, University of Opole, 48, Oleska Street, 45-052 Opole, Poland; teobald@uni.opole.pl (T.K.)
* Correspondence: makieievium@gmail.com or n.makieieva@po.edu.pl

Abstract

Cathinone and its synthetic derivatives are one of the most commonly used narcotics in the world. Some studies describe their antidepressant and smoking cessation potential, as well as cytostatic activity on several cancer cell lines. The literature presents a limited amount of data on the polymorphism in cathinones crystals, as well as on the correlation between aromaticity and crystal stability. This work aims to analyze the effect of the crystal structure on the nucleus-independent chemical shift (NICS) and the harmonic oscillator model of aromaticity (HOMA) values of bk-2C-B cathinone derivative polymorphs—EBIJOR and EBIJUX. A comparative analysis of NICS and HOMA values with an isolated drug molecules is also performed in this study. A higher aromaticity of molecules in polymorph EBIJOR was observed, compared to in EBIJUX. This may indicate a higher stability of EBIJOR compared to EBIJUX.

Keywords: cathinone; polymorphism; aromaticity

1. Introduction

Cathinone and its synthetic derivatives constitute one of the most popular groups of narcotics [1]. Low production costs and the ability to alter the spectrum and potency of its psychotropic properties by modifying the molecular skeleton of these substances have led to a rapid expansion of the list of cathinones on the drug market [2–5]. Consequently, methods for detecting these drugs in various matrices using different analytical techniques [6–10] and by correlating the chemical and biological properties of cathinones are becoming increasingly important [11,12]. The literature contains data on a wide range of toxic effects on various organs caused by cathinone use. The most common side effects are cardiotoxicity, hepatotoxicity, and neurotoxicity. Changes in the toxicity strength and spectrum with modifications of the cathinone structure have not yet been fully studied [13–22]. Furthermore, structural modifications lead to differences in the ability of cathinones to pass through various biological barriers (e.g., blood–lymph, blood–brain, or the cell membrane). Consequently, differences in the distribution and metabolism of different cathinones are observed [12,23–27]. In addition to their toxic side effects, the medicinal potential of selected cathinones is also worth mentioning. For example, bupropion is a registered antidepressant and a smoking cessation agent. Limited data are available on the potential of selected cathinones for the treatment of chronic fatigue and appetite suppression [28–31]. Therefore, expanding and correlating data on the chemical and biological properties of cathinones is

Check for updates

Academic Editors: Łukasz Szeleszczuk and Aidar T. Gubaidullin

Received: 8 August 2026
Revised: 21 August 2026
Accepted: 26 August 2026
Published: 28 August 2026

Copyright: © 2026 by the authors. Licensee MDPI, Basel, Switzerland. This article is an open access article distributed under the terms and conditions of the Creative Commons Attribution (CC BY) license.

important for obtaining a deeper understanding of the spectrum of possible toxic properties, as well as on their medicinal potential.

One of the important properties of organic and inorganic substances is their ability to form crystalline solids. In the physicochemical characterization of crystals, one of the key parameters is the potential polymorphism. This factor can play a key role in studying biological properties, as polymorphs can exhibit significantly different solubility in environments with different polarities and pH, variable melting point, hardness, stability, and a number of other parameters that play a significant role in biodistribution, biological activity, and the rate of metabolism of a substance in the organism [32]. In the case of cathinone and its synthetic derivatives, crystal polymorphism has been poorly described in the literature. During the preparation of this paper, only two articles focusing on polymorphism in ethylone and 2-amino-1-(4-bromo-2,5-dimethoxyphenyl)ethan-1-one (bk-2C-B) crystals were found in the Scopus database [33,34]. In the case of ethylone, the structures were determined using powder diffractometry [33]. Moreover, two polymorphs of bk-2C-B—EBIJOR and EBIJUX—have been described [34]. bk-2C-B polymorphs have become the subject of current research.

The molecular skeleton of cathinone and its derivatives contains a benzene ring. Consequently, their aromaticity may change under the influence of modification by substituents with different strengths of electron-donating/electron-withdrawing properties. It has been noted that the effect of increasing/decreasing aromaticity can play a role in changing the type and strength of interactions of the compound under study with various biomolecules, as well as its ability to participate in various biochemical transformations [35,36]. In the case of crystals, an increase in structure stability with an increase in the aromaticity of the participating molecules has been noted [37]. The influence of aromaticity localization on the crystal formation and its structure, as well as the electron transfer properties of the molecules in solid state have also been described [38]. Stabilization of the amorphous phase, prevention of recrystallization processes, and improvement of solubility in a polar environment (with a possible improvement in the bioavailability) were also observed for the anticancer drug enzalutamide co-amorphized with aromatic molecules [39]. Therefore, studying the aromaticity of molecules in crystals is important for determining both the physicochemical stability and biological potential of organic compounds. During the preparation of this work, no studies on the effects of aromaticity in cathinone crystals, or any attempts to correlate aromaticity with the thermodynamic stability of polymorphs, were found in the literature. Therefore, this study aims to expand existing knowledge on the aromaticity of bk-2C-B molecules in two polymorphic crystal forms. The information obtained may allow for a more detailed analysis of the relative stability of polymorphs EBIJOR and EBIJUX, which may be useful both in the context of the physicochemical characterization of the analyzed cathinone derivatives and potential changes in the bioavailability of this psychotropic compound consumed in different polymorphic forms.

2. Materials and Methods

Calculations were performed using Gaussian 16 C. 02 software (Gaussian, Inc., Wallingford, CT, USA) [40]. Density functional theory (DFT) was used for both the calculations of structural optimization and spectroscopic property calculations. The B3LYP density functional [41,42] was used with Grimme's empirical correction for dispersion, D3BJ [43]. This methodology was chosen to optimally capture weak intermolecular interactions in the crystal fragments with efficient use of computational resources. Due to the large size of the analyzed crystal fragments of the two bk-2C-B polymorphs, the Pople's 6-311++G** basis set [44,45] was used. All calculations were performed in the gas phase. Partial optimization was performed—only the lengths of bonds with the hydrogen atoms were optimized,

while maintaining the remaining structural parameters according to the crystallographic data [34]. NICS magnetic indexes were calculated as three individual parameters: chemical shift values in the center of the bk-2C-B benzene ring [NICS(0)]; chemical shift values 1 Å above the center of the benzene ring [NICS(1)]; and their Z-component [NICS(1)zz] [46]. The change in all aromaticity parameters in crystal fragments was estimated as the difference between the values for a cathinone derivative and a benzene and single bk-2C-B molecule (optimized on the B3LYPD3BJ/6-311++G** level of the theory in vacuum, see the Supplementary Materials). HOMA values were calculated according to the formula below:

$$HOMA = 1 - \frac{\alpha}{n}\sum_{i=1}^{n}\left(R_{opt} - R_i\right)^2 \quad (1)$$

where n is the number of bonds in the ring (n = 6 for benzene). α is an empirical normalization constant, individual to each bond type forming the ring. The benzene ring is formed by only CC type bonds, α = 257.7. R_{opt} is the reference bond length (in Å) in an "ideal aromatic" system. R_{opt} = 1.388 Å for the CC bond type [47,48]. R_i is the experimental bond length (in Å) for the analyzed bk-2C-B molecules [34,47,48]. Experimental crystal data were analyzed using Mercury 4.0 software (CCDC, Cambridge, UK) [49].

3. Results and Discussion

To analyze aromaticity in crystal structures closest to the experimental ones, this study utilized a single molecule and fragments of the crystal network of the EBIJOR and EBIJUX polymorphs of bk-2C-B, in which only the X-H bond lengths were optimized. Figure 1 shows the structure of 2-amino-1-(4-bromo-2,5-dimethoxyphenyl)ethan-1-one molecule with a water molecule and a chlorine anion. Since this study examines the crystal structure, the modeling was performed in vacuum. As can be seen from Figure 1, in the experimental data, bk-2C-B appears as the -NH^+ cation. Previous studies have noted difficulties in modeling the ionic forms of molecules in vacuum [50–53]. It was noted that a solution to this problem could be the addition of single water molecule near the charged fragments of the molecule [53,54]. For this reason, a discrete water molecule was also added in this study. Water molecules and chlorine/bromine ions were also present in the experimental crystal structure of both bk-2C-B polymorphs. Therefore, the positions of water and CI^- both in the single structure and in the fragments of both polymorphs are preserved according to the data of Power et al. [34].

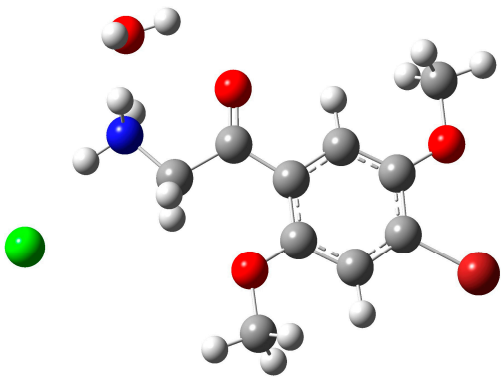


Figure 1. The structure of molecule bk-2C-B taken from the crystal network and partially optimized (with a single water molecule and chlorine anion).

In [34], from which the EBIJOR and EBIJUX experimental structures were taken, it was shown that the distribution of the Cl^- and Br^- ions is 70%:30%. Both anions were assigned with merged ellipsoids. Consequently, it was difficult to assign the positions of the chlorine

and bromine anions. Since Cl^- dominates in the crystal network, the Br^- positions were not considered in this study and all ion positions were surrounded by CI^-. Figure 2 shows fragments of the EBIJOR and EBIJUX crystals modeled in this study. The numbering of bk-2C-B molecules in both polymorphs is also shown to simplify further interpretation of the results.

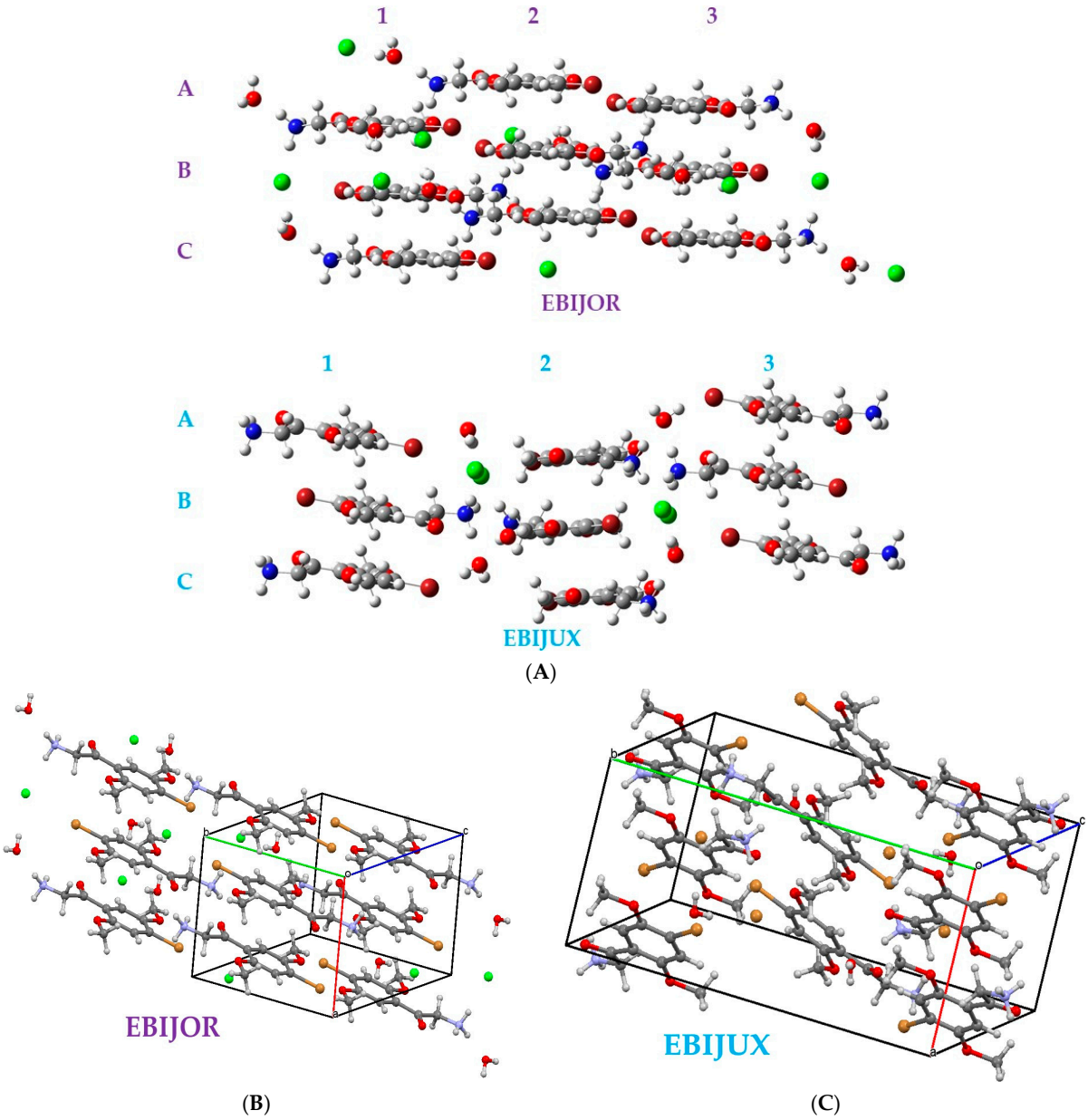


Figure 2. The structures of the EBIJOR and EBIJUX crystal fragments [34], partially optimized and analyzed in this study with (**A**) their molecular numbering, used to further interpret the results, and (**B**,**C**) the unit cells. EBIJOR has a P-1 space group, while EBIJUX has a $P2_1/n$ group.

The NICS and HOMA parameters are comparative, as the values for the analyzed ring are compared with data for a similar aromatic cycle. Therefore, to simplify tracking changes in NICS and HOMA values in molecules with different positions in the crystal fragment, comparative ΔNICS and ΔHOMA values were analyzed. ΔNICS was calculated as the difference between the NICS values for benzene or a single bk-2C-B molecule, minus the values for bk-2C-B rings in the crystal. ΔHOMA was calculated as the difference between the HOMA values for bk-2C-B rings in the crystal, minus the values for benzene or a single bk-2C-B molecule. Therefore, the increase in ΔNICS and ΔHOMA values corresponds to

an increase in aromaticity in the benzene ring of bk-2C-B in the crystal fragment. Figure 3 shows the ΔNICS values at different points from the bk-2C-B rings in two polymorphs compared to benzene, while Figure 4 provides comparative data with bk-2C-B molecule. The red curves represent data for molecules in polymorph EBIJOR, and the green curves represent data for molecules in polymorph EBIJUX.

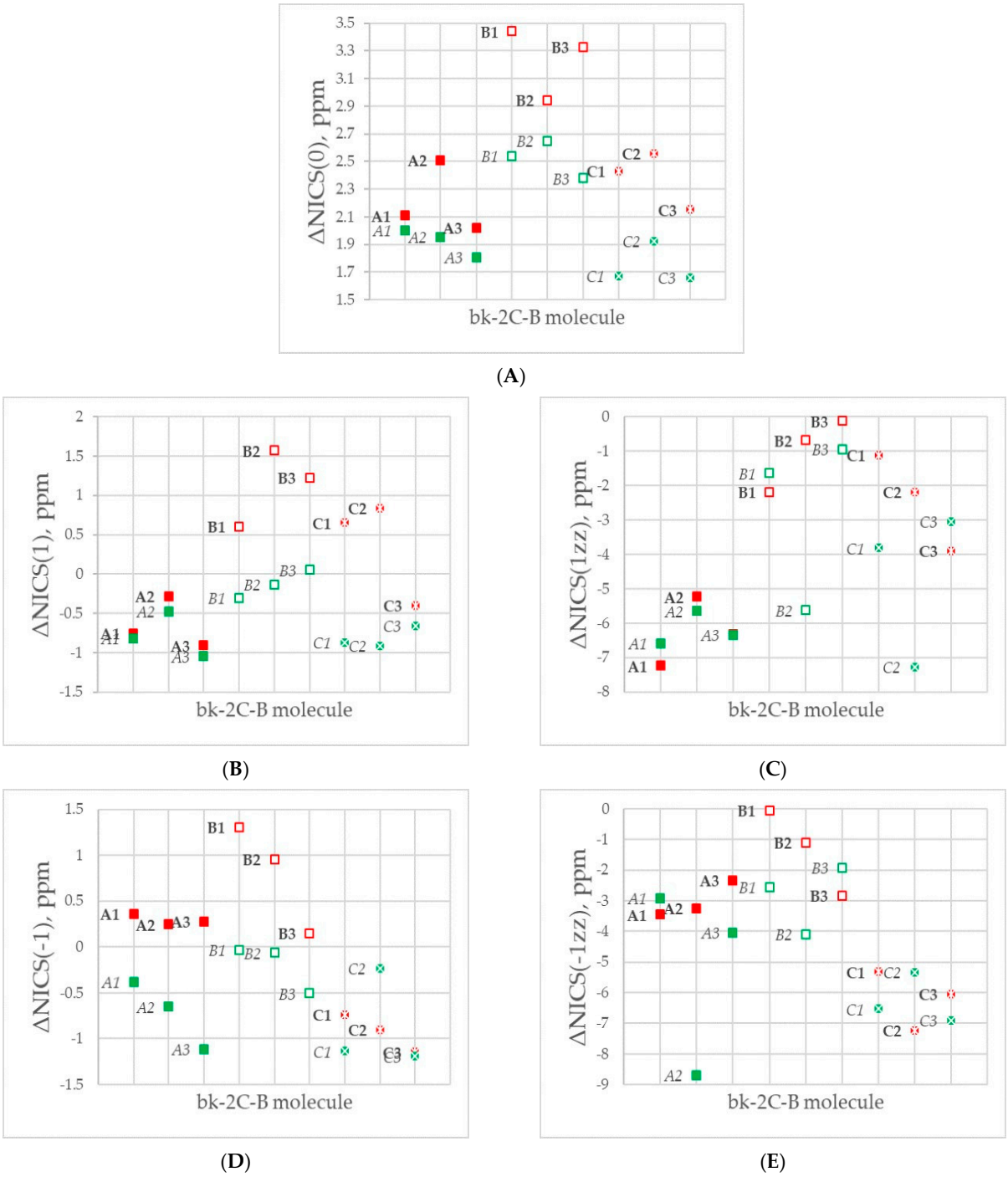


Figure 3. Relative values of the NICS parameters in bk-2C-B polymorphs (compared with benzene): (**A**) ΔNICS(0); (**B**,**C**) ΔNICS(1) and Z-component; and (**D**,**E**) ΔNICS(-1) and Z-component. The red symbols correspond to EBIJOR, and the green ones to the EBIJUX polymorph. Each point is labeled with the number of the corresponding molecule in the crystal fragment (according to Figure 2A).

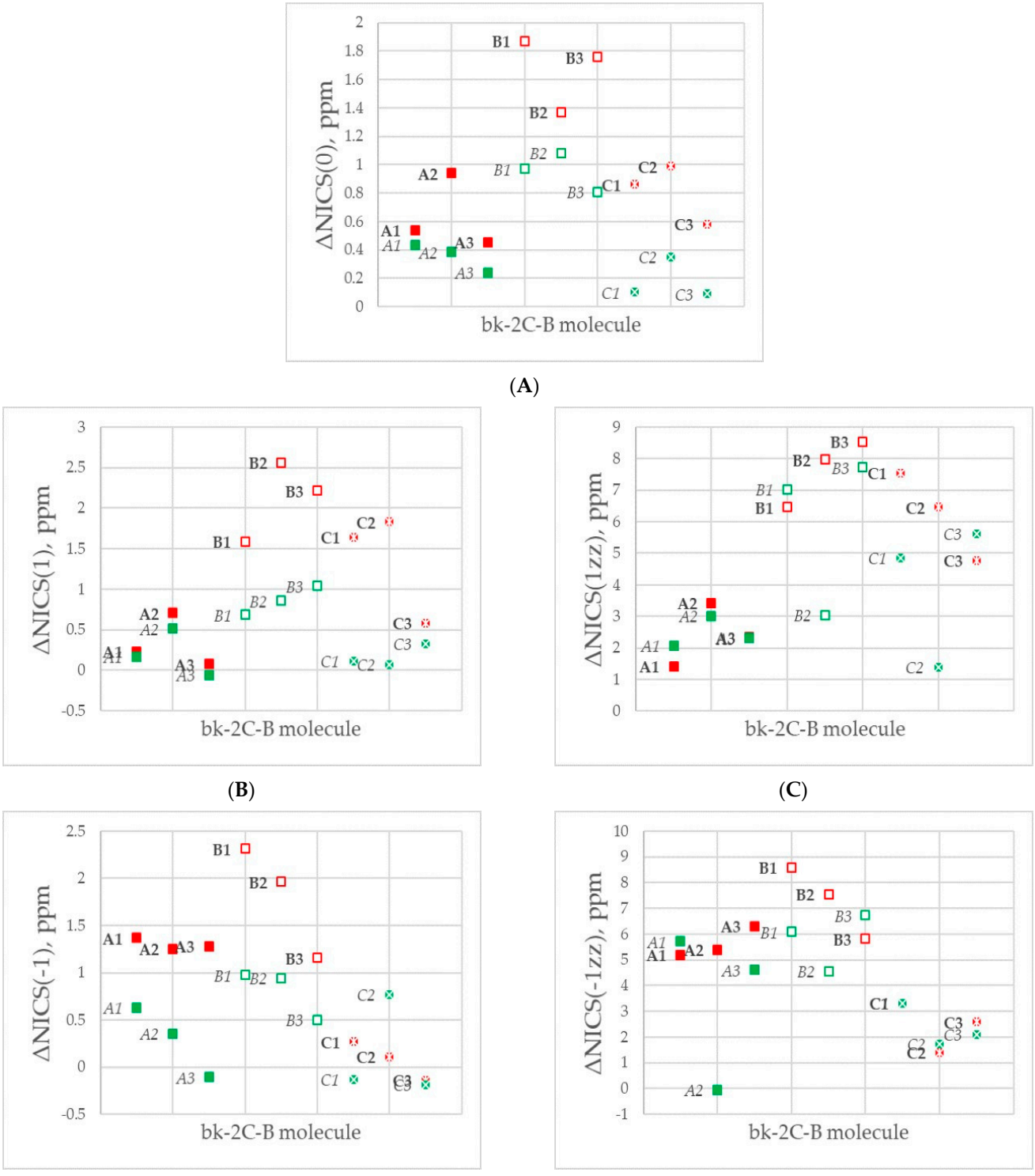


Figure 4. Relative values of the NICS parameters in bk-2C-B polymorphs (compared with a single bk-2C-B molecule): (**A**) ΔNICS(0); (**B**,**C**) ΔNICS(1) and Z-component; and (**D**,**E**) ΔNICS(-1) and Z-component. The red symbols correspond to EBIJOR, and the green ones to the EBIJUX polymorph. Each point is labeled with the number of the corresponding molecule in the crystal fragment (according to Figure 2A).

As can be seen from Figure 3A, in the case of the NICS parameter in the ring, an increase in values is observed for all molecules in polymorphs EBIJOR and EBIJUX compared to benzene. This trend can be explained as previously done by Portella et al. [55]: the

proximity of the aromatic rings leads to intermolecular π··π interactions overestimating the NICS(0) values. Therefore, the results obtained for polymorphs EBIJOR and EBIJUX should be interpreted with caution. However, it is worth noting that the increase in aromaticity was stronger for all molecules of polymorph EBIJOR compared to EBIJUX. Similar trends can also be seen in Figure 4A, where the NICS(0) data for both polymorphs were compared with molecule bk-2C-B. It could be noted that for both polymorphs (see Figures 3A and 4A), the increase in NICS(0) was greatest for molecules of the B series, i.e., the belt located between the two layers A and C. As a result, the B molecules of both polymorphs were subject to the greatest effect of intermolecular π··π interactions. In analyzing the ΔNICS(1) (see Figures 3B and 4B), it is worth noting that the values of this parameter were correlated with the position of the A-C layers of both polymorphs in the crystal fragments. Since this parameter was analyzed in the direction above the crystal network, in the case of the upper sphere A, the ΔNICS(1) values were characterized, compared to those of benzene, by a small decrease in aromaticity (Figure 3B) and, compared to molecule bk-2C-B, by a small increase in aromaticity for most rings of both polymorphs. However, in the case of EBIJOR, this increase was slightly greater than in EBIJUX. The molecules of layer B, located between layers A and C, were the most stabilized by π··π interlayer interactions. As a consequence, the increase in ΔNICS(1) compared to both benzene and bk-2C-B was maximal. In this case, a significant increase in aromaticity could be seen in polymorph EBIJOR compared to EBIJUX (see Figures 3B and 4B). In the next layer, C, the ΔNICS(1) values changed similarly to those for molecules B1-3. Since layer C was stabilized by only one upper layer of molecules bk-2C-B, the increase in aromaticity was smaller compared to layer B. The ΔNICS(1) data, compared with those for both benzene and bk-2C-B, are in agreement with most of the values of the Z-component 1 Å above the plane of the molecules in both polymorphs, ΔNICS(1zz) (see Figures 3C and 4C). Both of the ΔNICS(1) and ΔNICS(1zz) datasets demonstrate greater aromatic stabilization of bk-2C-B molecules in polymorph EBIJOR compared to EBIJUX. It is worth noting that the ΔNICS values 1 Å above the plane of the bk-2C-B molecules in the crystalline fragments are consistent with the 1 Å indices below the rings surface. As can be seen in Figures 3D,E and 4D,E, layer C exhibits the smallest increase in aromaticity, as it does not interact with bk-2C-B molecules 1 Å below the rings plane in the analyzed crystalline fragments. The greatest increase in aromaticity is observed in layer B, where the molecules are located between layers A and C, and the average increase is observed for molecules A1–A3 above layer B. In summary, based on the ΔNICS values at different positions relative to the benzene rings of bk-2C-B in the crystalline fragments, it could be suspected that polymorph EBIJOR is more stabilized by intermolecular π··π interactions. Further confirmation of this assumption could also be provided by the smaller distances between the benzene rings of bk-2C-B molecules in adjacent layers in EBIJOR compared to EBIJUX (see Table 1). This may serve as an additional factor for the greater stabilization of EBIJOR compared to EBIJUX. However, this assertion requires experimental confirmation.

To better understand the changes in aromaticity in the two bk-2C-B polymorphs, comparative HOMA data were also analyzed. Since the structure of the cathinone derivative is significantly substituted at various positions on the benzene ring, the comparison was made only relative to a single bk-2C-B molecule. As can be seen in Table 2, for both polymorphs, there is a small difference in aromaticity relative to the single cathinone molecule. However, a slight increase in aromaticity is noted in EBIJOR compared to EBIJUX. Although the differences were minor, due to the small effect of the local chemical environment in the crystal on the geometric parameters of the ring, consistency can be observed between the ΔNICS and ΔHOMA results.

Table 1. Distances (in Å, indicated by a dashed line) between bk-2C-B benzene rings in polymorphs EBIJOR and EBIJUX.

bk-2C-B Molecules [1]	EBIJOR	EBIJUX
A1··A2	3.3838	3.4743
A2··A3	3.3700	3.4275
B1··B2	3.3905	3.4868
B2··B3	3.3639	3.4454
C1··C2	3.3842	3.4601
C2··C3	3.3636	3.4247

[1] Molecules numbered according to Figure 2A.

Table 2. Relative values of HOMA parameters in bk-2C-B polymorphs compared with single bk-2C-B molecule.

bk-2C-B Molecule [1]	EBIJOR	EBIJUX
A1	0.00093	0.00010
A2	0.00091	-6.83678×10^{-5}
A3	0.00092	3.81439×10^{-5}
B1	0.00076	-1.48049×10^{-5}
B2	0.00093	−0.00014
B3	0.00076	1.23395×10^{-5}
C1	0.00093	0.00014
C2	0.00087	-4.8701×10^{-5}
C3	0.00094	-1.42079×10^{-5}

[1] Molecules numbered according to Figure 2A.

In analyzing both NICS and HOMA data trends, it can be seen that they jointly indicate a tendency toward greater aromatic stabilization of molecules in polymorph EBIJOR compared to EBIJUX. This effect may serve as an auxiliary factor to achieve the potentially higher physicochemical stability of a crystal stabilized by stronger total intramolecular aromaticity effects and intermolecular $\pi\cdot\cdot\pi$ interactions. However, this assumption requires more detailed experimental analysis supported by additional in silico studies. One of the effects affecting the accuracy of the obtained results is the difficulty in assigning the positions of the CI^- and Br^- ions based on available crystallographic structures. Consequently, intermolecular interactions and the associated effects of aromaticity changes were considered with a certain inaccuracy. Furthermore, the inclusion of larger crystal fragments than in this study, which would allow for a more accurate determination of changes in molecule aromaticity in different local chemical environments, requires significant computational resources. Consequently, further research is required to determine potential polymorphism in cathinone crystals, supported by high-level theoretical studies. Since we did not obtain permission to perform experimental work with cathinones during the preparation of this work, this study was limited to molecular modeling. The obtained results could be used as a theoretical basis for studying the stability of bk-2C-B polymorphs and similar cathinones under various physicochemical conditions, as well as for expanding our understanding of the relationship between aromaticity effects and the relative stability of cathinone polymorphs.

4. Conclusions

In this work, we study the changes in the aromaticity of bk-2C-B molecules in two polymorphic forms—EBIJOR and EBIJUX. This effect was studied for a partially optimized crystal structure using the magnetic aromaticity index (NICS) and the geometric aromaticity index (HOMA). The values of both parameters in different molecules of the crystal frag-

ments indicate an increase in aromaticity in EBIJOR compared to EBIJUX. This phenomenon may be caused by the combined effect of the internal electron density distribution with effective intermolecular $\pi \cdot\cdot \pi$ interactions. A higher aromatic stabilization in EBIJOR may serve as an auxiliary factor regarding the potentially higher physicochemical stability of this polymorph. However, this assumption requires additional experimental confirmation.

Supplementary Materials: The following supporting information can be downloaded at https://www.mdpi.com/article/10.3390/cryst16090562/s1: Table S1: Structures of benzene and bk-2C-B (with a water molecule and chlorine ion) with its two polymorphs (EBIJOR and EBIJUX) partially optimized (only X-H bond lengths) in vacuum at the B3LYPD3BJ/6-311++G** level of the theory with Gauss ghost atoms (Bq). All structures are optimized in the singlet form with total system charge "0" for bk-2C-B, EBIJOR, and benzene and "+5" for EBIJUX.

Author Contributions: Conceptualization, N.M., T.K., and K.E.; methodology, N.M., T.K., and K.E.; software, N.M.; validation, N.M., T.K., and K.E.; formal analysis, N.M., T.K., and K.E.; investigation, N.M.; resources, N.M.; data curation, N.M.; writing—original draft preparation, N.M.; writing—review and editing, N.M., T.K., and K.E.; visualization, N.M. All authors have read and agreed to the published version of the manuscript.

Funding: This research received no external funding.

Data Availability Statement: Data are contained within the article or Supplementary Materials. The original contributions presented in this study are included in the article/Supplementary Material. Further inquiries can be directed to the corresponding author.

Acknowledgments: Created using resources provided by Wroclaw Centre for Networking and Supercomputing (https://man.e-science.pl/pl/kdm/oprogramowanie/r (accessed on 1 August 2026)). Grant no. hpc-titanium-1721124296.

Conflicts of Interest: The authors declare no conflicts of interest.

References

1. de Ternay, J.; Plasse, A.; Rolland, B. The Rising Wave of Cathinone Use in People Attending Harm Reduction Facilities: A French Repeated Cross-Sectional Study (2019–2023). *Addict. Sci. Clin. Pract.* **2026**, *21*, 31. [CrossRef] [PubMed]
2. Van Hout, M.C. Kitchen Chemistry: A Scoping Review of the Diversionary Use of Pharmaceuticals for Non-Medicinal Use and Home Production of Drug Solutions. *Drug Test. Anal.* **2014**, *6*, 778–787. [CrossRef] [PubMed]
3. Archer, R.P. Fluoromethcathinone, a New Substance of Abuse. *Forensic Sci. Int.* **2009**, *185*, 10–20. [CrossRef] [PubMed]
4. Kehr, J.; Ichinose, F.; Yoshitake, S.; Goiny, M.; Sievertsson, T.; Nyberg, F.; Yoshitake, T. Mephedrone, Compared with MDMA (Ecstasy) and Amphetamine, Rapidly Increases Both Dopamine and 5-HT Levels in Nucleus Accumbens of Awake Rats. *Br. J. Pharmacol.* **2011**, *164*, 1949–1958. [CrossRef] [PubMed]
5. Smith, D.A.; Negus, S.S.; Poklis, J.L.; Blough, B.E.; Banks, M.L. Cocaine-like Discriminative Stimulus Effects of Alpha-Pyrrolidinovalerophenone, Methcathinone and Their 3,4-Methylenedioxy or 4-Methyl Analogs in Rhesus Monkeys. *Addict. Biol.* **2017**, *22*, 1169–1178. [CrossRef] [PubMed]
6. Liu, C.; Jia, W.; Li, T.; Hua, Z.; Qian, Z. Identification and Analytical Characterization of Nine Synthetic Cathinone Derivatives N-Ethylhexedrone, 4-Cl-Pentedrone, 4-Cl-α-EAPP, Propylone, N-Ethylnorpentylone, 6-MeO-Bk-MDMA, α-PiHP, 4-Cl-α-PHP, and 4-F-α-PHP. *Drug Test. Anal.* **2017**, *9*, 1162–1171. [CrossRef] [PubMed]
7. Vendrell-Dones, M.O.; Hernandez, E.; Dogruer Erkok, S.; McCord, B. Detection of Synthetic Cathinones in Seized Drugs Using Surface-Enhanced Raman Spectroscopy (SERS). *Forensic Chem.* **2024**, *41*, 100613. [CrossRef]
8. Zhao, L.; Qin, M.; Zheng, T.; Wu, G.; Lu, T. Carboxyl Hybrid Monolithic Column In-Tube Solid-Phase Microextraction Coupled with UPLC-QTRAP MS/MS for the Determination of Amphetamine-Type Stimulants. *J. Chromatogr. A* **2024**, *1737*, 465464. [CrossRef] [PubMed]
9. Sobue, Y.; Hotoda, K.; Ishii, A.; Kusakabe, K.; Ohta, J.; Takahashi, R.; Kato, N.; Sugaya, T.; Ishihara, K. New On-Site Color Test to Discriminate Cocaine and Cathinone Derivatives. *Sci. Justice* **2024**, *64*, 642–648. [CrossRef] [PubMed]
10. Reitzel, L.A.; Dalsgaard, P.W.; Müller, I.B.; Cornett, C. Identification of Ten New Designer Drugs by GC-MS, UPLC-QTOF-MS, and NMR as Part of a Police Investigation of a Danish Internet Company. *Drug Test. Anal.* **2012**, *4*, 342–354. [CrossRef] [PubMed]

11. Soares, J.; Costa, V.M.; Gaspar, H.; Santos, S.; de Lourdes Bastos, M.; Carvalho, F.; Capela, J.P. Structure-Cytotoxicity Relationship Profile of 13 Synthetic Cathinones in Differentiated Human SH-SY5Y Neuronal Cells. *NeuroToxicology* **2019**, *75*, 158–173. [CrossRef] [PubMed]
12. Lopes, R.P.; Miranda, C.C.; Fernandes, T.G.; Gaspar, H.; Antunes, A.M.M. The Cytotoxicity of Synthetic Cathinones on Dopaminergic-Differentiated SH-SY5Y Neuroblastoma Cell Line: Exploring the Role of β-Keto Metabolic Reduction. *Food Chem. Toxicol.* **2025**, *204*, 115658. [CrossRef] [PubMed]
13. Zawilska, J.B.; Wojcieszak, J. α-Pyrrolidinophenones: A New Wave of Designer Cathinones. *Forensic Toxicol.* **2017**, *35*, 201–216. [CrossRef]
14. Wojcieszak, J.; Andrzejczak, D.; Woldan-Tambor, A.; Zawilska, J.B. Cytotoxic Activity of Pyrovalerone Derivatives, an Emerging Group of Psychostimulant Designer Cathinones. *Neurotox. Res.* **2016**, *30*, 239–250. [CrossRef] [PubMed]
15. Leyrer-Jackson, J.M.; Nagy, E.K.; Olive, M.F. Cognitive Deficits and Neurotoxicity Induced by Synthetic Cathinones: Is There a Role for Neuroinflammation? *Psychopharmacology* **2019**, *236*, 1079–1095. [CrossRef] [PubMed]
16. Boulanger-Gobeil, C.; St-Onge, M.; Laliberté, M.; Auger, P.L. Seizures and Hyponatremia Related to Ethcathinone and Methylone Poisoning. *J. Med. Toxicol.* **2012**, *8*, 59–61. [CrossRef] [PubMed]
17. Warrick, B.J.; Wilson, J.; Hedge, M.; Freeman, S.; Leonard, K.; Aaron, C. Lethal Serotonin Syndrome After Methylone and Butylone Ingestion. *J. Med. Toxicol.* **2012**, *8*, 65–68. [CrossRef] [PubMed]
18. Daziani, G.; Lo Faro, A.F.; Montana, V.; Goteri, G.; Pesaresi, M.; Bambagiotti, G.; Montanari, E.; Giorgetti, R.; Montana, A. Synthetic Cathinones and Neurotoxicity Risks: A Systematic Review. *Int. J. Mol. Sci.* **2023**, *24*, 6230. [CrossRef] [PubMed]
19. Rodrigues, C.H.P.; Mariotto, L.S.; Castro, J.S.; Peruquetti, P.H.; Silva-Junior, N.C.; Bruni, A.T. Acute, Chronic, and Post-Mortem Toxicity: A Review Focused on Three Different Classes of New Psychoactive Substances. *Forensic Toxicol.* **2023**, *41*, 187–212. [CrossRef] [PubMed]
20. Frew, J.R.; Goodman, D.; Brunette, M. Perinatal Outcomes of Synthetic Cathinone ("Bath Salts") Use in Pregnancy: A Case Series. *J. Subst. Use* **2024**, *29*, 524–527. [CrossRef]
21. Valsalan, R.; Varghese, B.; Soman, D.; Buckmaster, J.; Yew, S.; Cooper, D. Multi-Organ Dysfunction Due to Bath Salts: Are We Aware of This Entity? *Intern. Med. J.* **2017**, *47*, 109–111. [CrossRef] [PubMed]
22. Kramer, C.L.; Wetzel, D.R.; Wijdicks, E.F.M. Devastating Delayed Leukoencephalopathy Associated with Bath Salt Inhalation. *Neurocrit Care* **2016**, *24*, 454–458. [CrossRef] [PubMed]
23. Fabregat-Safont, D.; Barneo-Muñoz, M.; Carbón, X.; Hernández, F.; Martinez-Garcia, F.; Ventura, M.; Stove, C.P.; Sancho, J.V.; Ibáñez, M. Understanding the Pharmacokinetics of Synthetic Cathinones: Evaluation of the Blood–Brain Barrier Permeability of 13 Related Compounds in Rats. *Addict. Biol.* **2021**, *26*, e12979. [CrossRef] [PubMed]
24. Grecco, G.G.; Kisor, D.F.; Magura, J.S.; Sprague, J.E. Impact of Common Clandestine Structural Modifications on Synthetic Cathinone "Bath Salt" Pharmacokinetics. *Toxicol. Appl. Pharmacol.* **2017**, *328*, 18–24. [CrossRef] [PubMed]
25. Wojcieszak, J.; Andrzejczak, D.; Kedzierska, M.; Milowska, K.; Zawilska, J.B. Cytotoxicity of α-Pyrrolidinophenones: An Impact of α-Aliphatic Side-Chain Length and Changes in the Plasma Membrane Fluidity. *Neurotox. Res.* **2018**, *34*, 613–626. [CrossRef] [PubMed]
26. Zhou, X.; Bouitbir, J.; Liechti, M.E.; Krähenbühl, S.; Mancuso, R.V. Para-Halogenation of Amphetamine and Methcathinone Increases the Mitochondrial Toxicity in Undifferentiated and Differentiated SH-SY5Y Cells. *Int. J. Mol. Sci.* **2020**, *21*, 2841. [CrossRef] [PubMed]
27. Pail, P.B.; Costa, K.M.; Leite, C.E.; Campos, M.M. Comparative Pharmacological Evaluation of the Cathinone Derivatives, Mephedrone and Methedrone, in Mice. *NeuroToxicology* **2015**, *50*, 71–80. [CrossRef] [PubMed]
28. Wilkes, S. The Use of Bupropion SR in Cigarette Smoking Cessation. *Int. J. Chronic Obstr. Pulm. Dis.* **2008**, *3*, 45–53. [CrossRef] [PubMed]
29. Fava, M.; Rush, A.J.; Thase, M.E.; Clayton, A.; Stahl, S.M.; Pradko, J.F.; Johnston, J.A. 15 Years of Clinical Experience with Bupropion HCl: From Bupropion to Bupropion SR to Bupropion XL. *Prim. Care Companion J. Clin. Psychiatry* **2005**, *7*, 106–113. [CrossRef] [PubMed]
30. Goldberg, J.; Gardos, G.; Cole, J.O. A Controlled Evaluation of Pyrovalerone in Chronically Fatigued Volunteers. *Int. Pharmacopsychiatry* **2017**, *8*, 60–69. [CrossRef] [PubMed]
31. Seaton, D.A.; Duncan, L.J.P.; Rose, K.; Scott, A.M. Diethylpropion in the Treatment of "Refractory" Obesity. *Br. Med. J.* **1961**, *1*, 1009–1011. [CrossRef] [PubMed]
32. Chistyakov, D.; Sergeev, G. The Polymorphism of Drugs: New Approaches to the Synthesis of Nanostructured Polymorphs. *Pharmaceutics* **2020**, *12*, 34. [CrossRef] [PubMed]
33. Maheux, C.R.; Alarcon, I.Q.; Copeland, C.R.; Cameron, T.S.; Linden, A.; Grossert, J.S. Identification of Polymorphism in Ethylone Hydrochloride: Synthesis and Characterization. *Drug Test. Anal.* **2016**, *8*, 847–857. [CrossRef] [PubMed]

34. Power, J.D.; Kavanagh, P.; O'Brien, J.; Barry, M.; Twamley, B.; Talbot, B.; Dowling, G.; Brandt, S.D. Test Purchase, Identification and Synthesis of 2-Amino-1-(4-Bromo-2, 5-Dimethoxyphenyl)Ethan-1-One (Bk-2C-B). *Drug Test. Anal.* **2015**, *7*, 512–518. [CrossRef] [PubMed]
35. Jezuita, A.; Makowska-Janusik, M.; Ejsmont, K.; Marczak, W. Substituent Effect in Histamine and Its Impact on Interactions with the G Protein-Coupled Human Receptor H1 Modelled by Quantum-Chemical Methods. *Molecules* **2025**, *30*, 3736. [CrossRef] [PubMed]
36. Travis, C.R.; Henriksen, H.C.; Wilkinson, J.R.; Schomburg, N.K.; Treacy, J.W.; Kean, K.M.; Houk, K.N.; Waters, M.L. WDR5 Binding to Histone Serotonylation Is Driven by an Edge–Face Aromatic Interaction with Unexpected Electrostatic Effects. *J. Am. Chem. Soc.* **2024**, *146*, 27451–27459. [CrossRef] [PubMed]
37. Fedyanin, I.V.; Voronin, A.A. Unusual Cation· · · cation Interactions in Pure and Mixed Zundel Salts of 4H-[1,2,3]Triazolo[4,5-c][1,2,5]Oxadiazole 5-Oxide. *Struct. Chem.* **2026**, *37*, 1165–1176. [CrossRef]
38. Yang, T.; Kong, X.; Wei, H.; Geng, L.; Li, Y. Thiophene-Fused Isomerism Governs Optoelectronic Properties, Crystal Packing, and Carrier-Transport Characteristics in Dodecyl-Substituted Angular Anthradithiophenes. *ACS Appl. Electron. Mater.* **2026**, *8*, 4461–4470. [CrossRef]
39. Chatziadi, A.; Neubergerová, K.; Balaga, V.K.R.; Trunov, D.; Šoóš, M. Selective Formation of Coamorphous Systems with Enzalutamide: Benzene Rings as Key Structural Features. *Eur. J. Pharm. Sci.* **2025**, *214*, 107281. [CrossRef] [PubMed]
40. Frisch, M.J.; Trucks, G.W.; Schlegel, G.E.; Scuseria, M.A.; Robb, J.R.; Cheeseman, G.; Scalmani, V.; Barone, G.A.; Petersson, H.; Nakatsuji, X.; et al. Gaussian 16 Revision C.02. 2019. Available online: https://gaussian.com/citation/ (accessed on 1 August 2026).
41. Becke, A.D. Density-Functional Exchange-Energy Approximation with Correct Asymptotic Behavior. *Phys. Rev. A* **1988**, *38*, 3098–3100. [CrossRef] [PubMed]
42. Lee, C.; Yang, W.; Parr, R.G. Development of the Colle-Salvetti Correlation-Energy Formula into a Functional of the Electron Density. *Phys. Rev. B* **1988**, *37*, 785–789. [CrossRef] [PubMed]
43. Grimme, S.; Ehrlich, S.; Goerigk, L. Effect of the Damping Function in Dispersion Corrected Density Functional Theory. *J. Comput. Chem.* **2011**, *32*, 1456–1465. [CrossRef] [PubMed]
44. Clark, T.; Chandrasekhar, J.; Spitznagel, G.W.; Schleyer, P.V.R. Efficient Diffuse Function-Augmented Basis Sets for Anion Calculations. III. The 3-21+G Basis Set for First-Row Elements, Li–F. *J. Comput. Chem.* **1983**, *4*, 294–301. [CrossRef]
45. Krishnan, R.; Binkley, J.S.; Seeger, R.; Pople, J.A. Self-consistent Molecular Orbital Methods. XX. A Basis Set for Correlated Wave Functions. *J. Chem. Phys.* **1980**, *72*, 650–654. [CrossRef]
46. Chen, Z.; Wannere, C.S.; Corminboeuf, C.; Puchta, R.; Schleyer, P.V.R. Nucleus-Independent Chemical Shifts (NICS) as an Aromaticity Criterion. *Chem. Rev.* **2005**, *105*, 3842–3888. [CrossRef] [PubMed]
47. Kruszewski, J.; Krygowski, T.M. Definition of Aromaticity Basing on the Harmonic Oscillator Model. *Tetrahedron Lett.* **1972**, *13*, 3839–3842. [CrossRef]
48. Krygowski, T.M.; Szatylowicz, H.; Stasyuk, O.A.; Dominikowska, J.; Palusiak, M. Aromaticity from the Viewpoint of Molecular Geometry: Application to Planar Systems. *Chem. Rev.* **2014**, *114*, 6383–6422. [CrossRef] [PubMed]
49. Macrae, C.F.; Sovago, I.; Cottrell, S.J.; Galek, P.T.A.; McCabe, P.; Pidcock, E.; Platings, M.; Shields, G.P.; Stevens, J.S.; Towler, M.; et al. Mercury 4.0: From Visualization to Analysis, Design and Prediction. *J. Appl. Cryst.* **2020**, *53*, 226–235. [CrossRef] [PubMed]
50. Addicoat, M.A.; Stefanovic, R.; Webber, G.B.; Atkin, R.; Page, A.J. Assessment of the Density Functional Tight Binding Method for Protic Ionic Liquids. *J. Chem. Theory Comput.* **2014**, *10*, 4633–4643. [CrossRef] [PubMed]
51. Bodo, E.; Mangialardo, S.; Ramondo, F.; Ceccacci, F.; Postorino, P. Unravelling the Structure of Protic Ionic Liquids with Theoretical and Experimental Methods: Ethyl-, Propyl- and Butylammonium Nitrate Explored by Raman Spectroscopy and DFT Calculations. *J. Phys. Chem. B* **2012**, *116*, 13878–13888. [CrossRef] [PubMed]
52. Gong, L.; Guo, W.; Xiong, J.; Li, R.; Wu, X.; Li, W. Structures and Stability of Ionic Liquid Model with Imidazole and Hydrogen Fluorides Chains: Density Functional Theory Study. *Chem. Phys. Lett.* **2006**, *425*, 167–178. [CrossRef]
53. Makieieva, N.; Kupka, T.; Rahmonov, O. Modelling of Cathinone–Carbon Nanotube Complexes' Stability: Theory with a Cancer Treatment Perspective. *Appl. Sci.* **2025**, *15*, 8892. [CrossRef]
54. Doskocz, M.; Roszak, S.; Majumdar, D.; Doskocz, J.; Gancarz, R.; Leszczynski, J. Theoretical Studies on the Mechanism of C−P Bond Cleavage of a Model α-Aminophosphonate in Acidic Condition. *J. Phys. Chem. A* **2008**, *112*, 2077–2081. [CrossRef] [PubMed]
55. Portella, G.; Poater, J.; Bofill, J.M.; Alemany, P.; Solà, M. Local Aromaticity of [n]Acenes, [n]Phenacenes, and [n]Helicenes (n = 1–9). *J. Org. Chem.* **2005**, *70*, 2509–2521. [CrossRef] [PubMed]

Disclaimer/Publisher's Note: The statements, opinions and data contained in all publications are solely those of the individual author(s) and contributor(s) and not of MDPI and/or the editor(s). MDPI and/or the editor(s) disclaim responsibility for any injury to people or property resulting from any ideas, methods, instructions or products referred to in the content.